Heliyon 7 (2021) e07026

Contents lists available at ScienceDirect

Heliyon

journal homepage: www.cell.com/heliyon

Research article

Long-range interaction effects on coupled excitable nodes: traveling waves and chimera state

Guy Blondeau Soh [a], Robert Tchitnga [a,b,*], Paul Woafo [c]

[a] Laboratory of Electronics, Automation and Signal Processing, Faculty of Science, Department of Physics, University of Dschang, P.O. Box 67, Dschang, Cameroon
[b] Institute of Surface Chemistry and Catalysis, University of Ulm, Albert-Einstein-Allee 47, 89081 Ulm, Germany
[c] Laboratory of Modeling and Simulation in Engineering, Biomimetics and Prototypes, Faculty of Science, University of Yaoundé I, P.O. Box 812, Yaoundé, Cameroon

ARTICLE INFO

Keywords:
Traveling waves
Multi-chimera state
Excitable behavior
Electrical synapse
Long-range interaction

ABSTRACT

In this paper, analytical and numerical studies of the influence of the long-range interaction parameter on the excitability threshold in a ring of FitzHugh-Nagumo (FHN) system are investigated. The long-range interaction is introduced to the network to model regulation of the Gap junctions or hemichannels activity at the connexins level, which provides links between pre-synaptic and post-synaptic neurons. Results show that the long-range coupling enhances the range of the threshold parameter. We also investigate the long-range effects on the network dynamics, which induces enlargement of the oscillatory zone before the excitable regime. When considering bidirectional coupling, the long-range interaction induces traveling patterns such as traveling waves, while when considering unidirectional coupling, the long-range interaction induces multi-chimera states. We also studied the difference between the dynamics of coupled oscillators and coupled excitable neurons. We found that, for the coupled system, the oscillation period decreases with the increasing of the coupling parameter. For the same values of the coupling parameter, the oscillation period of the Oscillatory dynamics is greater than the oscillation period of the excitable dynamics. The analytical approximation shows good agreement with the numerical results.

1. Introduction

In neural circuits, network operations and communication are supported by action potentials [1, 2]. The mechanism of generation of action potentials is a key component in the regulation of information flow [3] and it is initiated at the gap junction (GJ) level. For this reason, GJs have been regarded as an important component within the neuronal networks that underlie synchronous neuronal activity and field potential oscillations [4]. Soon after GJs were identified as structural and functional components of intercellular junctions, attempts were made to discover their protein makeup. Results showed that GJs are formed by the interaction of 2 hemichannels (HCs), one contributed by each of the adjacent cells [5, 6]. Each HC is composed of connexins in vertebrates or innexins in invertebrates [7, 8]. Gap junctions of identical HCs are known as homo-typic GJs, while those of different HCs are known as hetero-typic GJs [9, 10]. A human presents more than 20 different connexins species [11, 12]. They are all named after their predicted molecular weight, expressed in kilodaltons (e.g., connexing43 call Cx43, has a molecular weight of 43 kilodaltons). Gap junctions permit the intercellular diffusion of ions, metabolites, and cytoplasmic messenger molecules smaller than 1 kilodalton. This short route connection serves as a powerful cell function coordinator in complex tissues like the heart and brain. But HC activity can be regulated by phosphorylation [13, 14, 15], redox potential [16, 17, 18, 19], pH [20, 21], and other conditions [22]. Exposition to low extracellular $Ca2+$ concentration [22], mechanical stress [23], or positive membrane voltages [22] has been observed to increase the open probability of different Cx HCs. This regulation affects the membrane fluidity of the GJs [24].

However, studies regarding the transmission of the information taking into account the regulation of HC activity still lack, the same as the studies on the influence of this regulation on the chimera state [25, 26, 27, 28, 29, 30, 31]. Chimera state represents a peculiar collective behavior of coupled identical oscillators characterized by the coexistence of coherent or synchronized and incoherent or unsynchronized groups. After its discovery in 2002 by Kuramoto and Battogtokh [32], the chimera state has been investigated in several neuronal processes,

* Corresponding author at: Laboratory of Electronics, Automation and Signal Processing, Faculty of Science, Department of Physics, University of Dschang, P.O. Box 67, Dschang, Cameroon.
E-mail address: robert.tchitnga@eaphysud.org (R. Tchitnga).

https://doi.org/10.1016/j.heliyon.2021.e07026
Received 21 December 2020; Received in revised form 21 February 2021; Accepted 5 May 2021

and some particular patterns have been found such as multi-chimera [25, 33, 34] and traveling chimera [25, 35, 36, 37, 38, 39].

In this work, we will study the effects of the regulation of HC activity on the electrical current at the connexins level of electrical synapses. We hypothesized that a specific long-range parameter represents the regulation parameter of HC activity on the communication in the brain areas. It characterizes the coupling between cells at different sites. The variation of the long-range parameter can be related to the variation of the temperature or of the fluidity of the milieu, or redox potential, etc. In recent years, many studies on the effect of long-range interactions have been carried out on different approaches [40, 41]. It has been shown that long-range interactions have effects on calcium-wave propagation [42] or on chimera patterns [43, 44]. We will also study the difference between the dynamics of coupled oscillators [45] and coupled excitable neurons.

The aim of the present work is embedded in the following twofold questions, considering [46] in which the electrical coupling between neurons has been elaborated, and [42] in which long-range interaction has been defined:

- Firstly, what are the effects of long-range coupling on the generation of action potentials in the electrically coupled excited neurons? Furthermore, how do these action potentials differ from the ones of coupled oscillators?
- Secondly, how does long-range interaction influences the chimera state?

The paper is organized as follows: Section 2 introduces the mathematical model of long-range interaction. Section 3 describes the mathematical model of the threshold parameter of electrical coupling, considering long-range interaction and exploiting the FitzHugh-Nagumo (FHN) neuron model used for most of the studies in the literature. Section 4 and Section 5 study the effects of the long-range coupling on the bidirectional coupling and the unidirectional coupling respectively. In the concluding section, we summarize our main results, present possible applications, and discuss open problems.

2. Model description

While electrical synapses are known to be the target of the neuromodulatory transmitters, increasing evidence indicates that they are profoundly influenced by the activity of the networks in which they are embedded. It is in this order that the HC activity of transmission of the information could be affected. We use a long-range coupling to model this influence. The model of the long-range coupling between neurons j and k is given by the following relation [42, 47]:

$$\sigma(r) = \sigma_0 \frac{1-r}{r} r^{|k-j|} \tag{1}$$

In this relation, σ_0 represents the system's coupling parameter, and r defines the range of interaction. This r can represent the parameter that regulates the HC activity during the interaction. According to the nature of this regulation parameter, the long-range coupling could be optimal for the proper choice of the range r. For example, the human brain's suitable temperature is taken very near 37 °C [20]. Far from this value, it does not work conveniently.

The absolute value $|k-j|$ represents the measure of the distance between neurons j and k.

However, Eq. (1) is more adapted for $|k-j| \geq 2$ to ensure that the long-range would be equal to zero when $r \to 0$. To manage even the case of $|k-j| = 1$ we will consider in this work the following model of long-range:

$$\sigma(r) = \sigma_0 (1-r) r^{|k-j|}. \tag{2}$$

The model of Eq. (2) is similar to that of Eq. (1) when $|k-j| \geq 2$.

The graphical model of the long-range coupling is given by (Fig. 1) representing its variation with the range of interaction r and the distance $|k-j|$. It shows that the coupling between cells decreases gradually as the distance $|k-j|$ increases. For the same HC activity, the near neighbors' long-range coupling parameter is greater than that of far neighbors. This description characterizes that as the signals propagate in the milieu, the number of receptors in the considered cells decreases.

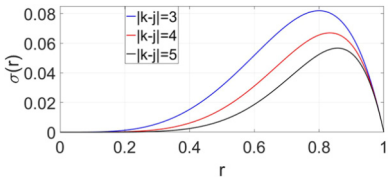

Fig. 1. Influence of the distance between neurons $|k-j|$ on the long-range coupling σ for $\sigma_0 = 1$. The long-range coupling decreases with the distance between neurons.

3. Mathematical model

3.1. Network model

In order to properly predict certain biological processes that are associated with the neuronal behavior, R. FitzHugh and J. Nagumo suggested the FitzHugh-Nagumo (FHN) model [2, 48]. It is an example of a relaxation model.

The mathematical form of the individual system describing the process of activation and deactivation dynamics of a spiking neuron is given by the following set of ordinary differential equations:

$$\begin{cases} b\dfrac{dx}{dt} &= x - \dfrac{x^3}{3} - y \\ \dfrac{dy}{dt} &= x + a \end{cases}. \tag{3}$$

Here x and y represent the activator (the membrane potential) and inhibitor (slow variable for current) variables. b is the small parameter characterizing the time scale separation of fast activator and slow inhibitor. In the present paper, we fix it at $b = 0.01$. The system exhibits limit cycle relaxation oscillations for the proper choice of the excitability threshold a. Otherwise, it exhibits either oscillatory behavior for $|a| < 1$ or excitable behavior for $|a| > 1$.

In the following parts, we assume identical elements in the excitable regime. We consider a network with a ring of non-locally coupled topology. In the network, we let N nodes be uniformly distributed on the ring and let each node be connected with its nearest neighbors. Each node represents a neuron where the interaction between two neurons can only be implemented through the connected connexins. The fluidity at the level of connexins is represented by the long-range coupling given below:

$$\begin{cases} b\dfrac{dx_j}{dt} &= x_j - \dfrac{x_j^3}{3} - y_j \\ &\quad + \dfrac{1}{2R}\displaystyle\sum_{k=j-R}^{j+R} \sigma(r)[b_{xx}(x_k - x_j) + b_{xy}(y_k - y_j)] \\ \dfrac{dy_j}{dt} &= x_j + a \\ &\quad + \dfrac{1}{2R}\displaystyle\sum_{k=j-R}^{j+R} \sigma(r)[b_{yx}(x_k - x_j) + b_{yy}(y_k - y_j)] \end{cases}. \tag{4}$$

Neuronal networks are often structured in topologies where strong interconnections between different neurons are found within a range R, but much fewer connections exist at longer distances [49, 50]. We approximate this feature by coupling with a strength $\sigma(r)$ within the R nearest neighbors from both sides. $2R$ is the total number of connections in the network for node j. Another important feature of Eq. (4) is that it contains not only direct $x-x$ and $y-y$ couplings, but also cross-couplings between the membrane potential (x) and the slow variable for current (y). For the sake of simplicity, a rotational coupling matrix depending on a single parameter ϕ has been defined [49, 51] to model this feature as:

$$B = \begin{pmatrix} b_{xx} & b_{xy} \\ b_{yx} & b_{yy} \end{pmatrix} = \begin{pmatrix} cos\phi & sin\phi \\ -sin\phi & cos\phi \end{pmatrix} with \phi \in [-\pi, \pi]. \tag{5}$$

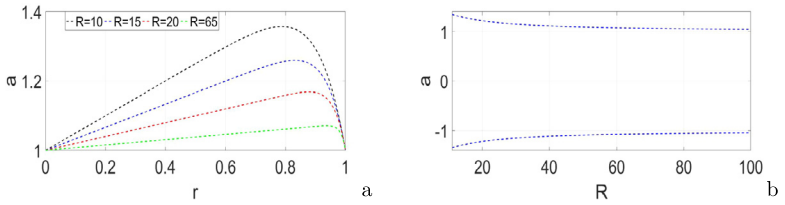

Fig. 2. Variation of the excitability threshold a, when $\sigma_0 = 5$, (a) with r, for $R = 10$ (black dashed line), $R = 15$ (blue dashed line), $R = 20$ (red dashed line), $R = 65$ (green dashed line), (b) with R for $r = 0.8$.

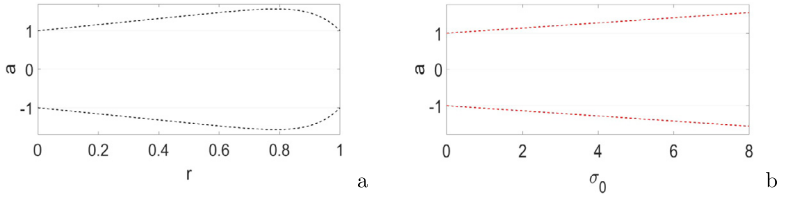

Fig. 3. Variation of the excitability threshold a, (a) with r for $R = 10$ and $\sigma_0 = 5$, (b) with σ_0 for $R = 10$ and $r = 0.8$.

In this section, we address the question of the influence of long-range coupling on the excitability threshold a by taking the parameter ϕ near to $\frac{\pi}{2}$ as suggested in [49]. For $\phi \simeq \frac{\pi}{2}$, $B = \begin{pmatrix} 0 & 1 \\ -1 & 0 \end{pmatrix}$,

Eq. (4) is reduced to:

$$\begin{cases} b\frac{dx_j}{dt} &= x_j - \frac{x_j^3}{3} - y_j + \frac{1}{2R}\sum_{k=j-R}^{j+R}\sigma(r)[(y_k - y_j)] \\ \frac{dy_j}{dt} &= x_j + a - \frac{1}{2R}\sum_{k=j-R}^{j+R}\sigma(r)[(x_k - x_j)] \end{cases}. \tag{6}$$

This yields the following approximation when considering only the node j in the network:

$$\begin{cases} b\frac{dx_j}{dt} &= x_j - \frac{x_j^3}{3} - y_j - y_j S(r) \\ \frac{dy_j}{dt} &= x_j + a + x_j S(r) \end{cases}, \tag{7}$$

with

$$S(r) = \frac{1}{2R}\sum_{k=j-R}^{j+R}\sigma(r) = \frac{\sigma_0}{R}r(1 - r^R). \tag{8}$$

The system exhibits either oscillatory behavior for $|a| < 1 + S(r)$ or excitable behavior for $|a| > 1 + S(r)$. The bifurcation points are obtained for each value of r, R and σ_0 by:

$$a = \pm(1 + \frac{\sigma_0}{R}r(1 - r^R)). \tag{9}$$

The maximum value of a for each value of R is obtained for:

$$r = \pm\sqrt[R]{\frac{1}{1+R}}. \tag{10}$$

The analytical result has revealed that by increasing R, the interval of values of a allowing oscillatory behavior is reduced (Fig. 2a), and its maximum is translated to the right way on $r-$line as presented in Fig. 2b. But whatever values of R and σ_0, the bifurcation point tends to 1 when r tends to 0 or when r tends to 1. By taking r values near to 0 or near to 1 the slopes at the right side in Fig. 3a and b decrease and are closed to $a = \pm 1$.

For the numerical simulation, we have considered a ring of neurons in which a signal can be reproduced after $N = 120$ neurons and thus the boundary conditions are taken to be cyclic and defined as $x(j+N) = x(j)$ and $y(j+N) = y(j)$.

Under random initials conditions and to be able to compare the analytical approximations' results (Fig. 3a) with those of numerical calculations (Fig. 4), we considered the following parameters' values: $b = 0.01$, $\phi = \frac{\pi}{2}$, $\sigma_0 = 17$, and $R = 5$. The maximum value of a is analytically equal to $a_{max} = 1.278$, obtained for $r = 0.8$. From Fig. 4a, when r tends to 0 or to 1, a is greater than the bifurcation value at this level, and the nodes are in an excitable state. By taking suitable values of r, values of a are less than the bifurcation value as seen in (Fig. 4b, c, d), so the nodes are in the oscillatory state after transition time from excitable state. The duration of transition decreases when r tends to its value corresponding to the bifurcation maximum value. The analytical approximation (Fig. 3a) is then in good agreement with the numerical interpretation (Fig. 4).

3.2. Period of network of neurons

This part aims to compare the oscillation period of a non-coupled oscillator and coupled oscillators for $|a| < 1$ with the oscillation period of coupled excitable neurons for $|a| > 1$.

Considering a single oscillator (Fig. 5), or coupled system (Fig. 6) for $|a| < 1$, the local dynamics are then periodically oscillating. The trajectories are linked to the nullcline at the right branch $B \to C$ (firing phase, from $x_+ = 2$ to $x_- = 1$) and at the left branch $D \to A$ (refractory phase, from $-x_+ = -2$ to $-x_- = -1$). The cycle approximated by four points A, B, C, and D corresponds to one period T. The approximation of the period for a single neuron when $|a| < 1$ is given by the following equation [52, 53]:

$$T_{so} = (a^2 - 1)\ln\frac{a^2 - 4}{a^2 - 1} + 3. \tag{11}$$

Where T_{so} denotes the period of single oscillator.

In the case of coupled oscillators when $|a| < 1$, the approximation of the period is given by the following equation [45]:

$$T_{co} = \frac{1}{(1+\sigma)^2}(x_+^2 - x_-^2 + (\frac{a^2}{(1+\sigma)^2} - 1)\ln\frac{a^2 - (1+\sigma)^2 x_+^2}{a^2 - (1+\sigma)^2 x_-^2}) \tag{12}$$

Where the parameter σ denotes the coupling strength, T_{co} is the period of coupled oscillators. The period T_{co} decreases with increasing of σ [45].

In the case of excitable dynamics, by example for $a = 1.35$, for a single neuron, the neuron does not oscillate, it stays constant at the value of a as shown in Fig. 4a. By coupling excitable neurons, it appears oscillation as shown in Fig. 7. However, contrarily for the precedents cases, the blue trajectory is not linked to the nullcline at the right branch $B \to C$ (firing phase) and the left branch $D \to A$ (refractory phase). The slow phases of the trajectory are separated from the nullcline by a certain gap. Since it is the coupling of excitable neurons, the trajectory starts to the value of $a = 1.35$, and performs a transient phase before

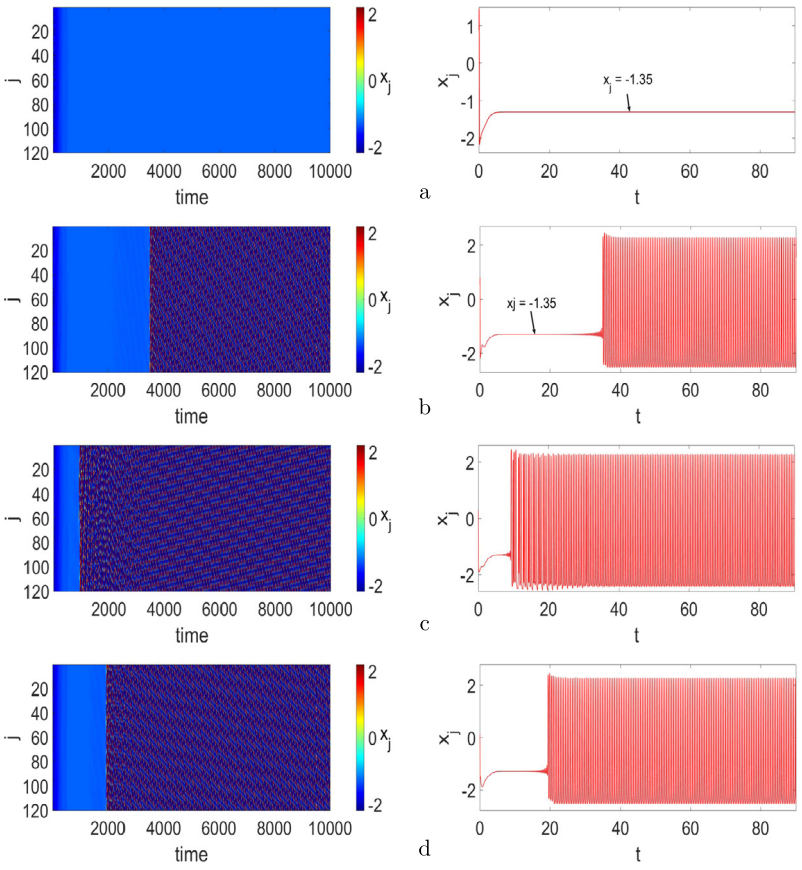

Fig. 4. Influence of the long-range coupling on the appearing of oscillations at the excitable state when $a = 1.27$, (a) for $r = 0.1$ or for $r = 0.98$, (b) for $r = 0.72$, (c) for $r = 0.8$, (d) for $r = 0.85$.

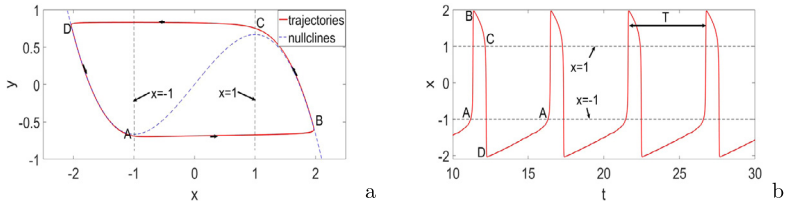

Fig. 5. (*a*) Phase portrait (trajectories in red line and nullclines in blue dashed line) of a single FitzHugh-Nagumo system and (*b*) the corresponding time series of activator $x(t)$ for $a = 0.1$.

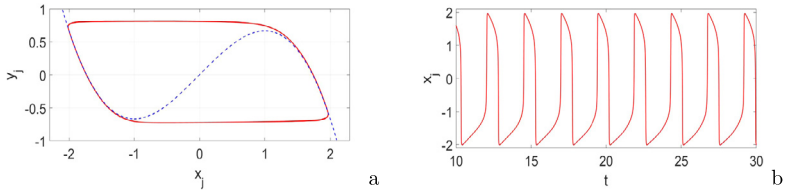

Fig. 6. (*a*) Phase portrait (trajectories in red line and nullclines in blue dashed line) of coupled oscillatory FitzHugh-Nagumo neurons and (*b*) the corresponding time series of activator $x_j(t)$ for $a = .35$.

adopting the permanent trajectory Fig. 8. The cycle approximated by four points A, B, C, and D corresponds to one period T.

In the following, we consider the excited coupled FHN system as described by Eq. (4). Its phase portrait and the corresponding time series of activator plotted in Fig. 7 are different from those of single neurons plotted in Fig. 5 and those of coupled oscillators plotted in Fig. 6. Nevertheless, the snapshot of each neuron of the system (Fig. 8) shows that each node spends the most significant part of its time in the firing ($B \to C$) and the refractory ($D \to A$) phases.

Similar to [45, 52, 53], we employ an analytic approximation for the period of neurons defined by Eq. (7) when $\phi \simeq \frac{\pi}{2}$. We have:

$$dt = \frac{1 - x_j^2}{(1 + S(r))^2 x_j + (1 + S(r))a} dx_j, \tag{13}$$

with $S(r)$ defined by Eq. (8).

One of the differences between coupled oscillators' dynamics and that of coupled excited neurons resides at the time series of activator $x_j(t)$ level. For the first case (Fig. 6b), oscillations are produced between

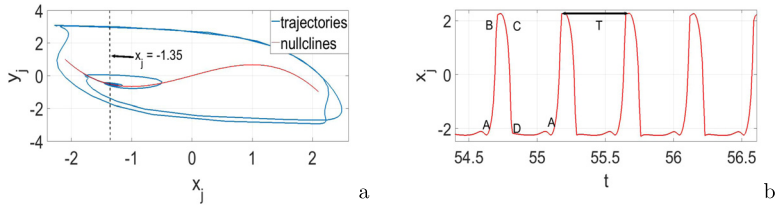

Fig. 7. (*a*) Phase portrait (trajectories in red line and nullclines in blue dashed line) of coupled excitable FitzHugh-Nagumo neurons and (*b*) the corresponding time series of activator $x_j(t)$ for $a = 1.35$.

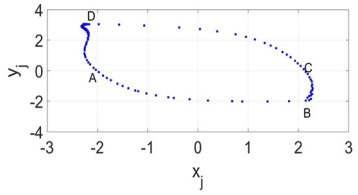

Fig. 8. Snapshot of coupled excitable FitzHugh-Nagumo neurons for $a = 1.35$.

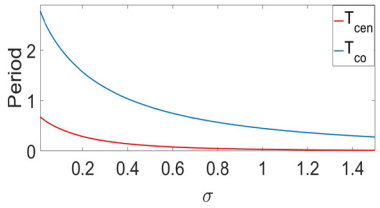

Fig. 9. Analytical approximations of the period for an FHN system. (a) Oscillatory dynamics for $a = 0.35$ (blue line), (b) excitable dynamics for $a = 1.35$ (red line).

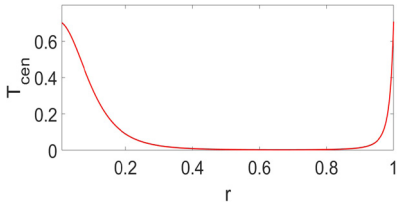

Fig. 10. Analytical approximations of the period of excitable coupled FHN in term of the long range parameter r for $a = 1.35$.

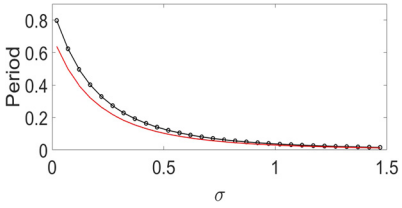

Fig. 11. Oscillation period of excitable coupled FHN in term of the coupling parameter for $a = 1.35$. Period obtained from numerical simulations (black circles), period obtained from analytical approximation of Eq. (16) (solid red line), period obtained from analytical approximation of Eq. (18) with the parameter $e = 0.22$ (solid black line).

± 2, that is why to express the period, authors of [45], for integration, used ± 2 as the maximum and the minimum.

For the second case (Fig. 7b), the maximum and the minimum are respectively greater than 2 and less than -2. We can integrate Eq. (13) analytically from $\pm x_+$ to $\pm x_-$ defined by $x_+ = 2 + \alpha$ and $x_- = 2$. α is the distance between the firing phase of the trajectory of uncoupled oscillators and coupled excitable neurons. It increases with increasing a, for the chosen value $a = 1.35$, $\alpha \simeq 0.23$. Let consider T_1 as a time of the firing phase and T_2 the time of the refractory phase:

$$T_1 = \int_{x_-}^{x_+} \frac{1-x_j^2}{(1+S(r))^2 x_j + (1+S(r))a} dx_j = \frac{1}{(1+S(r))^2} \int_{x_-}^{x_+} \frac{1-x_j^2}{x_j + \frac{a}{(1+S(r))} dx_j}, \text{ or}$$

$$T_1 = \frac{1}{(1+S(r))^2}\left(\frac{x_+^2 - x_-^2}{2} + \left(\frac{a^2}{(1+S(r))^2} - 1\right) \ln \frac{a - (1+S(r))x_+}{a - (1+S(r))x_-} - \frac{a}{1+S(r)}\right), \tag{14}$$

and $T_2 = \int_{-x_+}^{-x_-} \frac{1-x_j^2}{(1+S(r))^2 x_j + (1+S(r))a} dx_j = \frac{1}{(1+S(r))^2} \int_{-x_+}^{-x_-} \frac{1-x_j^2}{x_j + \frac{a}{(1+S(r))} dx_j}$, or

$$T_2 = \frac{1}{(1+S(r))^2}\left(\frac{x_+^2 - x_-^2}{2} + \left(\frac{a^2}{(1+S(r))^2} - 1\right) \ln \frac{a + (1+S(r))x_+}{a + (1+S(r))x_-} + \frac{a}{1+S(r)}\right). \tag{15}$$

The time duration of one cycle of a coupled excitable neuron when we neglect the fast motions $A \to B$ and $C \to D$ is then given by $T_{cen} = T_1 + T_2$:

$$T_{cen} = \frac{1}{(1+S(r))^2}(x_+^2 - x_-^2 + \left(\frac{a^2}{(1+S(r))^2} - 1\right) \ln \frac{a^2 - (1+S(r))^2 x_+^2}{a^2 - (1+S(r))^2 x_-^2}), \tag{16}$$

where T_{ceo} denotes the period of coupled excited neurons.

The analytical approximations of the period for an FHN system in the case of coupled oscillators (blue line) and of coupled excitable neurons (red line) are plotted in Fig. 9 considering the coupling parameter ($S(r) = \sigma$) constant. It comes out from Fig. 9 and from [45, 52, 53] that for the same value of $a \in]-1, 1[$, the oscillation period of a single oscillator (T_{so}) is greater than the oscillation period of coupled ones (T_{co}). For the coupled system (oscillatory or excitable states), the oscillation period decreases when σ increases. For the same values of σ the oscillation period of the Oscillatory dynamics (T_{co}) is greater than the oscillation period of the excitable dynamics (T_{cen}). This analytical approximation is in good agreement with the numerical results from Figs. 5b, 6b, 7b.

It is important to notice that, the amplitude of the time series of activator $x_j(t)$ of coupled excitable neurons increases as a increases far from ± 1.

The analytical approximations of the period of excitable coupled FHN in term of the long-range parameter r are plotted in Fig. 10. The oscillation period firstly decreases for the range of r from 0_+ to 0.8 which corresponds to the interval where the coupling parameter increases. Secondly, from $r \simeq 0.8$ until $r \simeq 1$, the oscillation period increases which corresponds to the interval where the coupling parameter decreases.

However, as in [52, 53], the transition from the left to the right branch or from the right to the left branch is not directly made. To account for the delay of transition, authors of [52, 53] modified the period of Eq. (11) by introducing a small parameter e as follows:

$$T = ((a^2 - 1) \ln |\frac{a^2 - 4}{a^2 - 1}| + 3)(1 + e). \tag{17}$$

In the light of the above, our expression of the period becomes:

$$T_{cen} = \frac{1}{(1+S(r))^2}(x_+^2 - x_-^2 + \left(\frac{a^2}{(1+S(r))^2} - 1\right) \ln \frac{a^2 - (1+S(r))^2 x_+^2}{a^2 - (1+S(r))^2 x_-^2})(1 + e). \tag{18}$$

In Fig. 11, we compare the analytical results with numerical simulations of the excitable coupled FHN system. For $a = 1.35$, and for $e = 0.22$, the analytical approximation (Solid red line) is in good agreement with the numerical results (black circles).

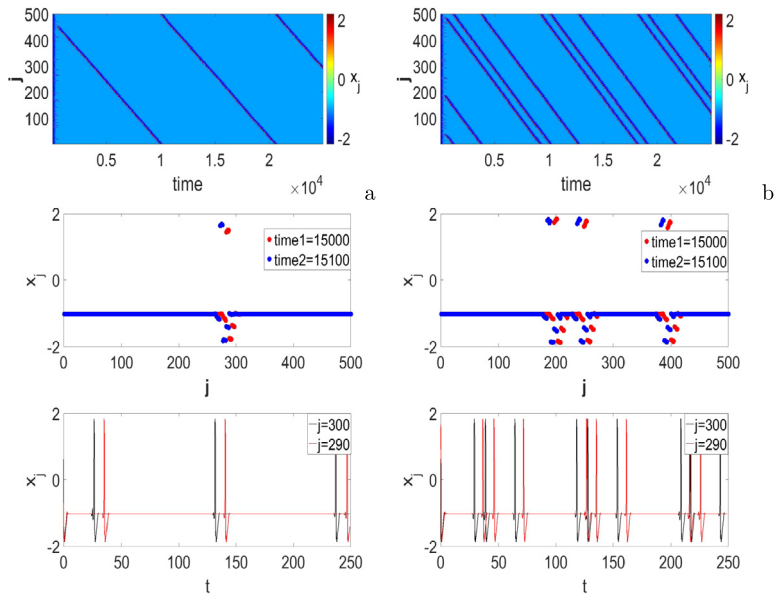

Fig. 12. Traveling wave by increasing the long-range r. (a) For $r = 0.53$ and (b) for $r = 0.54$.

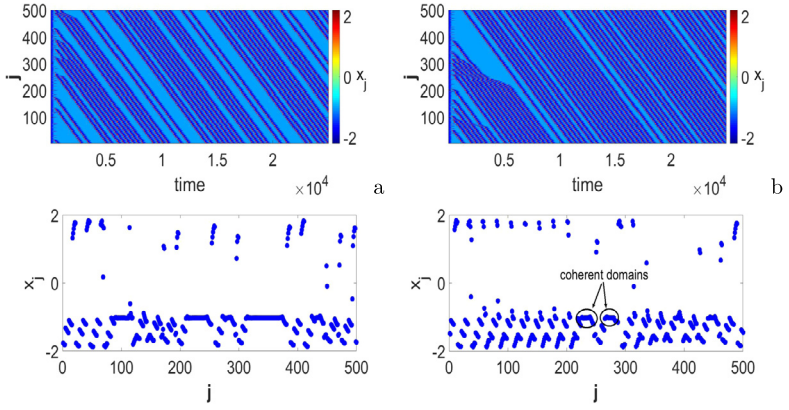

Fig. 13. Traveling patterns generated by increasing the long-range r. Panels present the space-time plot of the node variables x_j and their corresponding snapshot. (a) For $r = 0.55$, (b) for $r = 0.56$.

4. Effect of the range of interactions on the bidirectional coupling

In this section, we study the influence of the long-range parameter in the system described by Eq. (4). Elements are in excitable dynamics and parameters are set as $N = 500$, $a = 1.02$ and $\phi = \frac{\pi}{4} - 0.1$.

Fig. 12 is made of two columns for $r = 0.53$ (a), and $r = 0.54$ (b). In the first row, the space-time plot of the node variables x_j is depicted, and their corresponding snapshot at two different time $time_1 = 15000$ (red color) and $time_2 = 15100$ (blue color) are figured out in the second row. The last row presents the times series of the membrane potential x_j at the nodes $j = 290$ (red color) and $j = 300$ (black color). We can see that nodes are organized into spatial traveling groups of elements, interrupted by regions of oscillating elements that travel from the last to the first node. As the moving fronts on the panels indicate, the velocity of the oscillating regions around the ring increases with r.

The time series confirm the traveling behavior for two different times. Since incoherent domains are moving from the right side to the left, the node $j = 300$ oscillates before the node $j = 290$. Even looking at the snapshot panels of the node variables x_j at two different times, $time_1 = 15000$ (red color) and $time_2 = 15100$ (blue color), the incoherent behaviors in red are at the right side of the incoherent behaviors in blue. That is with respect to the time of the snapshot. The increasing of r facilitates the generation of new incoherent regions, and the number of spikes that form the spatial profile of the wave increases. It is to notice that those incoherent domains travel around the ring using a constant velocity [26, 31], as clearly indicated by the corresponding space-time plot.

For greater values of r, the area of traveling coherent regions decreases while the number of traveling waves increases. This traveling patterns behavior is illustrated by the Fig. 13. The area of the coherent regions in Fig. 13b for $r = 0.56$, is smaller than the area of the coherent regions in Fig. 13a for $r = 0.55$.

We found in Fig. 13 the traveling patterns in which the proportion of coherent domain is reduced when r increases. It is on this base that the coherent domains disappear; from $r = 0.58$, the whole system becomes completely unsynchronized. It starts to form the oblique stripes, and another typical pattern of traveling waves appears as shown in Fig. 14.

We conclude from the above results that long-range coupling takes a key role in the formation of different traveling patterns of Eq. (4).

5. Effect of the range of interactions on the unidirectional coupling

In this section, we study the influence of the long-range parameter in the system unidirectionally coupled described by Eq. (19). Elements are in excitable dynamics and parameters are set to $N = 500$, $a = 1.02$ and $\phi = \frac{\pi}{4} - 0.1$.

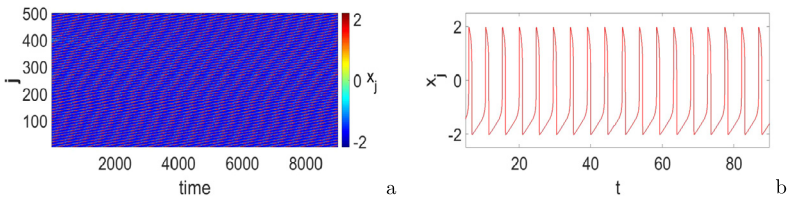

Fig. 14. Traveling action potential for $r = 0.7$. (a) The space-time plot of the node variables x_j. (b) The times series of membrane potential x_j.

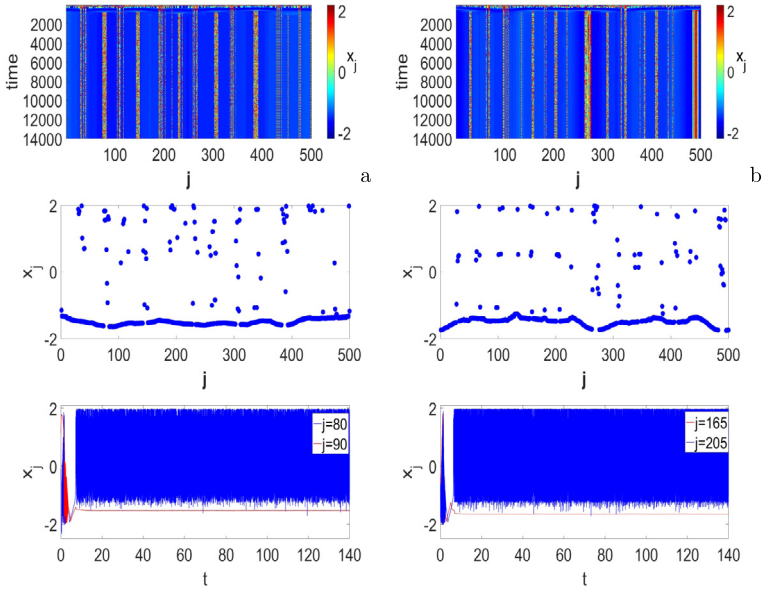

Fig. 15. Multi-chimera states. (a) For $r = 0.53$. (b) for $r = 0.54$.

$$\begin{cases} b\dfrac{dx_j}{dt} &= x_j - \dfrac{x_j^3}{3} - y_j \\ &+ \dfrac{1}{R}\displaystyle\sum_{k=j}^{j+R} \sigma(r)[b_{xx}(x_k - x_j) + b_{xy}(y_k - y_j)] \\ \dfrac{dy_j}{dt} &= x_j + a \\ &+ \dfrac{1}{R}\displaystyle\sum_{k=j}^{j+R} \sigma(r)[b_{yx}(x_k - x_j) + b_{yy}(y_k - y_j)] \end{cases} \tag{19}$$

Fig. 15 has two columns for $r = 0.53$ (left side), and $r = 0.54$ (right side). In the first row, the space-time plot of the node variables x_j is presented, and their corresponding snapshot at the time $time_1 = 12000$ is depicted in the second row. The last row presents the times series of membrane potential x_j. We can see that nodes are organized into coherent groups of elements, separated by regions of incoherent elements. This behavior of the coexistence of multiple synchronized and unsynchronized regions is well known as the multi-chimera states.

6. Conclusion

The main objective of this work was to investigate the dynamic of excitable coupled FitzHugh-Nagumo oscillators in a ring for which we have introduced the long-range interactions. We have reported how the long-range interactions can modify the excitability threshold a in an electrical coupled excitable neurons for each coupled parameter σ_0. For an appropriate choice of the rotational coupling matrix, the position of the maximum of a for each coupled neuron j on the $r - line$ depends only on the number of neurons R which are coupled to j. The above results are in accordance with the results of the (Fig. 4) presenting the influence of the long-range coupling on the appearing of oscillations at the excitable state. We also study the difference between the dynamics of coupled oscillators and coupled excitable neurons. We found that, for the coupled system (oscillatory or excitable states), the oscillation period decreases with the increasing of σ. For the same values of σ the oscillation period of the Oscillatory dynamics (T_{co}) is greater than the oscillation period of the excitable dynamics (T_{cen}). The analytical approximation is in good agreement with the numerical results. We also demonstrated that the combination of the parameter ϕ and the long-range interaction r can produce different traveling patterns such as traveling waves in the case of bidirectional coupling and multi-chimera in the case of unidirectional coupling.

These findings strongly suggest that the long-range coupling applied to the neurons' activities could play a critical role in the dynamics of cerebral activities.

Declarations

Author contribution statement

Guy Blondeau Soh: Performed the experiments; Analyzed and interpreted the data; Contributed reagents, materials, analysis tools or data; Wrote the paper.

Robert Tchitnga: Conceived and designed the experiments; Analyzed and interpreted the data; Contributed reagents, materials, analysis tools or data; Wrote the paper.

Paul Woafo: Conceived and designed the experiments; Wrote the paper.

Funding statement

This research did not receive any specific grant from funding agencies in the public, commercial, or not-for-profit sectors.

Data availability statement

No data was used for the research described in the article.

Declaration of interests statement

The authors declare no conflict of interest.

Additional information

No additional information is available for this paper.

References

[1] J.C. Sàez, V.M. Berthoud, M.C. Branes, A.D. Martinez, E.C. Beyer, Plasma membrane channels formed by connexins: their regulation and functions, Physiol. Rev. 83 (2003) 1359–1400.

[2] T. Klausberger, P. Somogyi, Neuronal diversity and temporal dynamics: the unity of hippocampal circuit operations, Science 321 (2008) 53–57.

[3] B.P. Bean, The action potential in mammalian central neurons, Nat. Rev. Neurosci. 8 (2007) 451–465.

[4] A. Posłuszny, The contribution of electrical synapses to field potential oscillations in the hippocampal formation, Front. Neural Circuits 8 (2014) 1–13.

[5] M. Vinken, T. Vanhaecke, P. Papeleu, S. Snykers, T. Henkens, V. Rogiers, Connexins and their channels in cell growth and cell death, Cell. Signal. 18 (2006) 592–600.

[6] M. Vinken, E. Decrock, E. De Vuyst, R. Ponsaerts, C. D'hondt, G. Bultynck, L. Ceelen, Connexins: sensors and regulators of cell cycling, Biochim. Biophys. Acta 1815 (2011) 13–25.

[7] M. Maes, E. Decrock, B. Cogliati, A.G. Oliveira, P.E. Marques, M.L. Dagli, G.B. Menezes, G. Mennecier, L. Leybaert, T. Vanhaecke, Connexin and pannexin (hemi)channels in the liver, Front. Physiol. 4 (2014) 1–8.

[8] M. Vinken, E. Decrock, L. Leybaert, G. Bultynck, B. Himpens, T. Vanhaecke, V. Rogiers, Non-channel functions of connexins in cell growth and cell death, Biochim. Biophys. Acta 8 (2012) 1818–2002.

[9] P. Liu, B. Chen, R. Mailler, Z.W. Wang, Antidromic-rectifying gap junctions amplify chemical transmission at functionally mixed electricalchemical synapses, Nat. Commun. 8 (2017) 1–16.

[10] M. Zancan, T. Malysz, D.J. Moura, A.M. Morás, L. Steffensand, A.A. Rasia Filho, Gap junctions and expression of cx36, cx43 and cx45 in the posterodorsal medial amygdala of adult rats, Histol. Histopathol. 35 (2020) 395–403.

[11] J. von Maltzahn, C. Euwens, K. Willecke, G. Söhl, The novel mouse connexin39gene is expressed in developing striated muscle Willeckeand, J. Cell Sci. 117 (2004) 5381–5392.

[12] X. Gong, C. Cheng, C. Xia, Connexins in lens development and cataractogenesis, J. Membr. Biol. 218 (2007) 9–12.

[13] X. Bao, S.C. Lee, L. Reuss, G.A. Altenberg, Change in permeant size selectivity by phosphorylation of connexin 43 gap-junctional hemichannels by pkc, Proc. Natl. Acad. Sci. USA 104 (2007) 4919–4924.

[14] J.L. Solan, P.D. Lampe, Key connexin 43 phosphorylation events regulate the gap junction life cycle, J. Membr. Biol. 217 (2007) 35–41.

[15] C. Puebla, B.A. Cisterna, D.P. Salas, F. Delgado-Lòpez, P.D. Lampe, J.C. Sàez, Linoleic acid permeabilizes gastric epithelial cells by increasing connexin 43 levels in the cell membrane via a gpr40- and akt-dependent mechanism, Biochim. Biophys. Acta 1861 (2016) 439–448.

[16] J.E. Contreras, H.A. Sanchez, E.A. Eugenin, D. Speidel, M. Theis, K. Willecke, Metabolic inhibition induces opening of unapposed connexin 43 gap junction hemichannels and reduces gap junctional communication in cortical astrocytes in culture, Proc. Natl. Acad. Sci. USA 99 (2002) 495–500.

[17] M.A. Retamal, Connexin and pannexin hemichannels are regulated by redox potential, Front. Physiol. 5 (2014) 1–9.

[18] M.A. Retamal, C.J. Cortés, L. Reuss, M.V. Bennett, J.C. Sàez, S-nitrosylation and permeation through connexin 43 hemichannels in astrocytes: induction by oxidant stress and reversal by reducing agents, Proc. Natl. Acad. Sci. USA 103 (2006) 4475–4480.

[19] M.A. Retamal, K.A. Schalper, K.F. Shoji, M.V. Bennett, J.C. Sàez, Opening of connexin 43 hemichannels is increased by lowering intracellular redox potential, Proc. Natl. Acad. Sci. USA 104 (2007) 8322–8327.

[20] D.L. Beahm, J.E. Hall, Hemichannel and junctional properties of connexin 50, Biophys. J. 82 (2002) 2016–2031.

[21] C. D'hondt, J. Iyyathurai, M. Vinken, V. Rogiers, L. Leybaert, B. Himpens, Regulation of connexin- and pannexin-based channels by posttranslational modifications, Biol. Cell 105 (2013) 373–398.

[22] J.C. Sàez, M.A. Retamal, D. Basilio, F.F. Bukauskas, M.V. Bennett, Connexin-based gap junction hemichannels: gating mechanisms, Biochim. Biophys. Acta 1711 (2005) 215–224.

[23] C. D'hondt, R. Ponsaerts, H. De Smedt, G. Bultynck, B. Himpens, Pannexins, distant relatives of the connexin family with specific cellular functions?, BioEssays 31 (2009) 953–974.

[24] M.L. Schultz, L. Tecedor, E. Lysenko, S. Ramachandran, C.S. Stein, B.L. Davidson, Modulating membrane fluidity corrects batten disease phenotypes in vitro and in vivo, Neurobiol. Dis. 115 (2018) 182–193.

[25] G.B. Soh, P. Louodop, R. Kengne, R. Tchitnga, Chimera dynamics in an array of coupled Fitzhugh-Nagumo system with shift of close neighbors, Heliyon 6 (2020) e03739.

[26] E.A. Martens, S. Thutupalli, A. Fourriere, O. Hallatschek, Chimera states in mechanical oscillator networks, Proc. Natl. Acad. Sci. USA 110 (2013) 10563–10567.

[27] D.B. Strukov, G.S. Snider, D.R. Stewart, The missing memristor found, Nature 453 (2008) 80–83.

[28] M. Itoh, L.O. Chua, Memristor oscillators, Int. J. Bifurc. Chaos 18 (2008) 3183–3206.

[29] B.C. Bao, J.P. Xu, Z. Liu, Initial state dependent dynamical behaviors in a memristor based chaotic circuit, Chin. Phys. Lett. 27 (2010) 1–3.

[30] C.B. Tabi, A.S. Etémé, A. Mohamadou, Unstable discrete modes in Hindmarsh-Rose neural networks under magnetic flow effect, Chaos Solitons Fractals 123 (2019) 116–123.

[31] N.D. Tsigkri-DeSmedt, J. Hizanidis, E. Schöll, P. Hövel, A. Provata, Chimeras in leaky integrate-and-fire neural networks: effects of reflecting connectivities, Eur. Phys. J. B 90 (2017) 1–11.

[32] Y. Kuramoto, D. Battogtokh, Coexistence of coherence and incoherence in nonlocally coupled phase oscillators, Nonlinear Phenom. Complex Syst. 5 (2002) 380–385.

[33] P. Hövel, I. Omelchenko, Multi-chimera states in Fitzhugh-Nagumo oscillators, BMC Neurosci. 14 (2013) 303.

[34] N.D. Tsigkri-DeSmedt, J. Hizanidis, P. Hövel, A. Provata, Multi-chimera states and transitions in the leaky integrate-and-fire model with nonlocal and hierarchical connectivity, Eur. Phys. J. Spec. Top. 225 (2016) 1149–1164.

[35] C. Tian, L. Hongjie, X. Kesheng, L. Zonghua, Chimera states in neuronal networks with time delay and electromagnetic induction, Nonlinear Dyn. 93 (2018) 1695–1704.

[36] O. Omel'chenko, Traveling chimera states, J. Phys. A, Math. Theor. 52 (2019) 104001–104011.

[37] A. Mishra, S. Saha, C. Hens, P. Roy, M. Bose, P. Louodop, H. Cerdeira, S. Dana, Coherent libration to coherent rotational dynamics via chimeralike states and clustering in a Josephson junction array, Phys. Rev. E 95 (2017) 010201.

[38] B.K. Bera, D. Ghosh, T. Banerjee, Imperfect traveling chimera states induced by local synaptic gradient coupling, Phys. Rev. E 94 (2016) 012215.

[39] A. Alvarez-Socorro, M. Clerc, N. Verschueren, Traveling chimera states in continuous media, Commun. Nonlinear Sci. Numer. Simul. 94 (2021) 105559–105568.

[40] J. Gross, F. Schmitz, I. Schnitzler, K. Kessler, K. Shapiro, B. Hommel, A. Schnitzler, Modulation of long-range neural synchrony reflects temporal limitations of visual attention in humans, Proc. Natl. Acad. Sci. USA 101 (2004) 13050–13055.

[41] P. Richerme, Z. Gong, A. Lee, C. Senko, S. Michalakis, A.V. Gorshkov, C. Monroe, Non-local propagation of correlations in quantum systems with long-range interactions, Nature 511 (2014) 198201.

[42] W.D. Kepseu, P. Woafo, Long-range interaction effects on calcium-wave propagation, Phys. Rev. E 78 (2008) 011922.

[43] D. Viennot, L. Aubourg, Quantum chimera states, Phys. Lett. A 380 (2016) 678–683.

[44] T. Banerjee, P.S. Dutta, A. Zakharova, E. Schöll, Chimera patterns induced by distance-dependent power-law coupling in ecological networks, Phys. Rev. E 94 (2016) 032206.

[45] J. Sawicki, I. Omelchenko, A. Zakharova, E. Schöll, Delay-induced chimeras in neural networks with fractal topology, Eur. Phys. J. B 92 (2019) 54.

[46] S. Majhi, M. Perc, D. Ghosh, Chimera states in uncoupled neurons induced by a multilayer structure, Sci. Rep. 6 (2016) 1–10.

[47] P. Woafo, T.C. Kofane, A.S. Bokosah, Kink static properties in a discrete ϕ^4 chain with long-range interactions, Phys. Rev. B 48 (1993) 10153–10159.

[48] J. Nagumo, S. Arimoto, S. Yoshizawa, An active pulse transmission line simulating nerve axon, Proc. IRE 50 (1962) 2061–2070.

[49] I. Omelchenko, O. Omel'chenko, P. Hövel, E. Schöll, When nonlocal coupling between oscillators becomes stronger: patched synchrony or multichimera states, Phys. Rev. Lett. 110 (2013) 224101.

[50] J.A. Henderson, P.A. Robinson, Geometric effects on complex network structure in the cortex, Phys. Rev. Lett. 107 (2011) 018102.

[51] A. Vüllings, J. Hizanidis, I. Omelchenko, P. Hövel, Clustered chimera states in systems of type-i excitability, New J. Phys. 16 (2014) 123039.

[52] E. Schöll, G. Hiller, P. Hövel, M.A. Dahlem, Time-delayed feedback in neurosystems, Philos. Trans. R. Soc. A 367 (2009) 1079–1096.

[53] S. Brandstetter, M.A. Dahlem, E. Schöll, Interplay of time-delayed feedback control and temporally correlated noise in excitable systems, Philos. Trans. R. Soc. A 368 (2010) 391–421.